jove

Real-time Analysis of Gut-brain Neural Communication: Cortex wide Calcium Dynamics in Response to Intestinal Glucose Stimulation

Serika Yamada[1], **Hiromu Monai**[1]

[1] Department of Biology, Faculty of Science, Ochanomizu University

Corresponding Author

Hiromu Monai
monai.hiromu@ocha.ac.jp

Citation

Yamada, S., Monai, H. Real-time Analysis of Gut-brain Neural Communication: Cortex wide Calcium Dynamics in Response to Intestinal Glucose Stimulation. *J. Vis. Exp.* (202), e65902, doi:10.3791/65902 (2023).

Date Published

December 29, 2023

DOI

10.3791/65902

URL

jove.com/video/65902

Abstract

Communication between the gastrointestinal tract and the brain after nutrient absorption plays an essential role in food preference, metabolism, and feeding behaviors. Particularly concerning specific nutrients, many studies have elucidated that the assimilation of glucose within gut epithelial cells instigates the activation of many signaling molecules. Hormones such as glucagon-like peptide-1 are renowned as quintessential signaling mediators. Since hormones predominantly influence the brain through circulatory pathways, they slowly modulate brain activity.

However, recent studies have shown two expeditious gut-brain pathways facilitated by the autonomic nervous system. One operates via the spinal afferent neural pathway, while the vagus nerve mediates the other. Consequently, brain responses following glucose assimilation in the gastrointestinal tract are complicated. Moreover, as intestinal stimulation finally induces diverse cortical activities, including sensory, nociceptive, reward, and motor responses, it is necessary to employ methodologies that facilitate the visualization of localized brain circuits and pan-cortical activities to comprehend gut-brain neural transmission fully. Some studies have indicated precipitous alterations in calcium ion (Ca^{2+}) concentrations within the hypothalamus and ventral tegmental area independently through different pathways after intestinal stimulation. However, whether there are changes in cerebral cortex activity has not been known.

To observe cerebral cortex activity after intragastric glucose injection, we developed an imaging technique for real-time visualization of cortex wide Ca^{2+} dynamics through a fully intact skull, using transgenic mice expressing genetically encoded Ca^{2+} indicators. This study presents a comprehensive protocol for a technique designed to monitor intestinal stimulation-induced transcranial cortex wide Ca^{2+} imaging following intragastric glucose injection via an implanted catheter. The preliminary data suggest

that administering glucose solution into the gut activates the frontal cortex, which remains unresponsive to water administration.

Introduction

Primarily, gut sensing of glucose occurs via the sweet taste receptors (Tas1r2, Tas1r3) and the sodium-glucose cotransporter 1 (SGLT-1) located in enteroendocrine cells within the intestinal lumen[1,2,3,4,5,6]. The sensation of glucose in the brain is a process that typically spans from minutes to hours after its absorption from the gut, an occurrence principally based on increased levels of plasma blood sugar and the release of hormones[7,8,9,10,11] (e.g., glucagon-like peptide-1 [GLP-1], Peptide YY (PYY), and glucose-dependent insulinotropic polypeptide [GIP]). They reach the arcuate nucleus of the hypothalamus (ARC), where they bind pro-opiomelanocortin (POMC) neurons and agouti-related protein (AgRP) neurons by blood flow and vagus nerve (parasympathetic nerve)[12,13,14]. The change in the activity of these neurons leads to control of metabolism and feeding behavior[15,16].

Recent literature increasingly highlights the significance of gut-brain neural signaling following glucose absorption. This complex pathway can be broadly categorized into two primary mechanisms. The first involves the activation of spinal afferents, ultimately influencing AgRP neuronal activity in the ARC. The second mechanism entails stimulation of the vagus nerve through connections with epithelial cells. Given the multifaceted ways gut epithelial cells can activate the vagus nerve[13], its role is considered versatile.

A significant proportion of gut vagus and spinal afferent nerve activities are associated with feeding behaviors[17,18,19]. However, emerging evidence suggests that certain vagus nerve fibers, projecting to "neuropod cells," are implicated in glucose preference. Neuropod cells, a subset of enteroendocrine cells, express SGLT-1 on their luminal side and convey sensory stimuli to a vagus nerve via glutamatergic synapses[2,20,21,22]. Activation of the vagus nerve triggers dopaminergic neurons in the ventral tegmental area (VTA) within seconds[19]. Notably, inhibiting vagal activation, particularly in the duodenum, using a glutamate antagonist reduces sucrose preference in mice[1]. This underscores the critical role of neuropod cell activation in modulating food choice behavior post-glucose intake[2].

Despite these advancements, a thorough understanding of the rapid intestinal glucose sensing mechanisms and their effect on cortical activities remains a complex enigma. Though brain activation controlled by AgRP neurons does not include the cerebral cortex[23], it is known that dopaminergic neurons in the VTA project to the cerebral cortex. However, whether rapid VTA dopaminergic neuronal activation after glucose sensing truly activates the cerebral cortex is unknown. To elucidate this mechanism, we investigated the potential for intragastric glucose administration to rapidly influence cortical Ca^{2+} dynamics in transgenic mice expressing a genetically encoded calcium indicator.

This paper presents a low-cost and less invasive method to comprehensively understand the changes in cortical activity following intragastric glucose administration using cortex wide Ca^{2+} imaging in mice Recently, the transcranial cortex wide Ca^{2+} imaging technique through an intact skull, using transgenic mice expressing genetically encoded calcium indicators, has gained popularity[24]. Notably, the BAC GLT-1-

G-CaMP7 #817 transgenic mouse line (also known as G7NG817 mouse) employed in this study expresses the Ca^{2+} sensor, G-CaMP7, in neurons and astrocytes[25]. Due to its high expression density in the cerebral cortex, this transgenic mouse line is especially suitable for transcranial cortex wide Ca^{2+} imaging using a standard epifluorescence microscope.

Protocol

All experimental protocols were approved by the Institutional Animal Care and Use Committee of Ochanomizu University, Japan (animal study protocols 22017). All animal experiments were performed according to the guidelines for animal experimentation of Ochanomizu University that conform with the Fundamental Guidelines for Proper Conduct of Animal Experiment and Related Activities in Academic Research Institutions (Ministry of Education, Culture, Sports, Science and Technology, Japan). Efforts were taken to minimize the number of animals used. This study was carried out in compliance with the ARRIVE guidelines.

1. Preparation of transgenic mice

1. To follow this experiment, use adult male and female BAC GLT-1-G-CaMP7 #817 transgenic mouse line, namely G7NG817 mice[24,25] (older than 8 weeks). The background strain of G7NG817 mice[25] is C57BL/6J.
2. House the mice under a 12 h /12 h light/dark cycle and raise them in groups of up to five mice.

2. Catheter creation

1. Use scissors to adjust the silicon tube (inner diameter 0.5 mm, outer diameter 1.0 mm) to a precise length of 7 cm (**Figure 1A-a**).
2. Adhere diminutive plastic beads (inner diameter 3 mm, outer diameter 5 mm) to the tailored tube, ensuring they are situated 3 mm from its terminus (**Figure 1A-b**). Affix the beads securely using cyanoacrylate glue (medical or standard variants are acceptable).
3. Excise a 23 G needle's apex and subsequently cut 1.5 cm from the needle tip (**Figure 1A-c**).
4. Introduce the sectioned 23 G needle from step 2.3 into the silicon tube's extremity, opposite to where the beads were affixed (**Figure 1A-d**).

3. Injector creation

1. Use pliers to excise 1 cm from the needle tip (**Figure 1B-a**).
   NOTE: Ensure the orifice at the severed end retains its integrity and does not get deformed, as any distortion could obstruct the injection solution's flow.
2. Couple the adapted 23 G injection needle from step 3.1.1 to a 2.5 mL syringe (**Figure 1B-b**).
3. Segment a silicon tube to the requisite length (a 15 cm silicon tube in this experiment) and sheath it over the 23 G injection needle (**Figure 1B-c**).
   NOTE: The volume of solution dispensed will fluctuate based on the tubing's length. For instance, with a 15 cm tube, approximately 50 µL of solution will linger post experiment.
4. Sever the 23 G injection needle 1.5 cm from the needle tip.
5. Join the sectioned portion from step 3.4 with the silicon catheter fashioned in step 3.3 (**Figure 1B-d**).
   NOTE: Ensure the orifices created in steps 3.1 and 3.4 remain undistorted post incision. If rectification is needed, employ pliers to restore its circular configuration.

4. Gastric localization

1. Administer anesthesia to the mouse via 3.0% isoflurane inhalation in a specified chamber.
2. Delicately transfer the anesthetized mouse from the inhalation chamber to the surgical table upon verifying the mouse's anesthetized state.
3. Lay the mouse supine, aligning its mouth proximate to the inhalation apparatus, and modulate the isoflurane concentration from 3.0% to 2.0%.
   NOTE: Disengage the inferior segment of the isoflurane mask from its superior counterpart and anchor the separated mask (upper segment) to the surgical table using adhesive tape.
4. Supplement the mouse's oral cavity, forelimbs, and hindlimbs to the surgical table using adhesive tape.
   NOTE: By fixing the mouse to the table, surgical errors due to movement can be prevented even if the mouse is anesthetized.
5. Remove the mouse's hair from the upper left abdomen by using depilatory cream.
6. Make a skin incision roughly 1.5 cm in length (**Figure 1C-b**), situated 1 cm to the right of the abdominal median and 5 mm below the xiphoid process (**Figure 1C-c**). Then, create a 1.5 cm incision in the abdominal wall at the same location as the initial skin incision.
   NOTE: Exercise caution to avoid inflicting harm to the underlying liver.
7. Delicately reposition the left hepatic lobe laterally using blunt-ended forceps, revealing the stomach beneath.

5. Catheter insertion

1. Elevate the stomach and cautiously extricate it through the incision.
   NOTE: Exercise utmost care to preserve the integrity of adjacent organs, notably the liver, and refrain from exerting undue force on the stomach.
2. Use scissors to create a diminutive perforation (approximately 1.5mm in diameter) in the pyloric antrum.
3. Introduce the catheter's terminus into the perforation, ensuring the bead is in direct contact with the pyloric antrum.
4. Adhere the catheter's bead to the stomach employing medical-grade cyanoacrylate glue.
   NOTE: Ensure the stomach remains unattached to surrounding organs.
5. Verify the firm attachment of the catheter to the stomach, then delicately reposition the stomach to its innate locale beneath the left hepatic lobe.
6. Stitch the abdominal wall, permitting the catheter to extend externally, using a 5/0 silk suture. After that, close the skin incision in a manner analogous to the abdominal closure.
7. Sterilize the operated region with 70% ethanol.
8. Gently reposition the mouse in a sanitized cage.
   NOTE: Postoperative mice should be singularly housed.
9. Allow a minimum recovery period of 48 h in a standard environment.

6. Preparation for *in vivo* transcranial Ca^{2+} imaging

1. Administer anesthesia to the mouse using isoflurane (induction at 2%; maintenance between 0.8% and 1.0%).
2. Secure the mouse onto a stereotaxic platform using auxiliary ear bars to mitigate the effects of pulsation and respiration. Subsequently, position the mouse under a fluorescence stereo microscope.
3. Employ a wideband blue fluorescence filter set (with excitation at 460-490 nm and emission at 520 nm) in conjunction with a mercury light source.
4. Capture the images using a camera and process them using the designated imaging software.
5. Carefully remove the hair from the scalp using an electric shaver or hair removal cream.
   NOTE: If using a razor, ensure that it is thoroughly disinfected and be careful not to cut the skin.
6. Disinfect the surface of the scalp using a cotton swab or similar tool with a solution of chlorhexidine gluconate diluted to 0.1-0.5%.
7. Apply a local anesthetic gel and wait for 5-10 min.
8. Prepare to apply dental acrylic cement.
   1. Use scissors to cut the scalp. Either completely remove the scalp or make a straight cut from the back of the head to the forehead.
   2. Use clips to expose the skull by extending any excess skin.
   3. Use a cotton swab to remove the connective tissue of the periosteum.
   4. Immediately apply the acrylic cement after removing the periosteum. Act quickly to prevent the skull surface from becoming opaque due to evaporation from the exposed bone.
   5. Wait for about 5 min for the cement to dry.

7. Transcranial Ca^{2+} imaging with intraduodenal glucose administration

1. Equilibrate both the experimental solution and saline to ambient temperature. Subject the mice to a dietary restriction for a specified duration (e.g., 2 h).
2. Purge any residual content within the mouse-side catheter using ~0.03 mL of saline before initiating the injection.
3. Aspirate the experimental solution (for instance, a 10% glucose solution prepared in 300 µL of water, complemented with an additional 300 µL of water) into the syringe, then interface it to the catheter. Ascertain the optimal dosage of the solution tailored to the specific experimental objective.
   NOTE: During this phase, exercise caution to prevent undue strain on the catheter, which might jeopardize the mouse's internal anatomy. Endeavor to manipulate the mouse-side tubing with utmost gentleness. Additionally, ensure the syringe remains devoid of air post solution aspiration, as entrapped air and bubbles could induce gastrointestinal distension.
4. Assess the mouse's physiological state and activate the imaging software's recording function by clicking on the **recording process** button of the software application.
5. Capture images at a resolution of **512 x 512 pixels, 16 bit** depth, and a **frame rate** of **10 Hz**.
   NOTE: The recording parameters can be adjusted to align with specific experimental requirements.

6. Acquire spontaneous data (e.g., spanning 50 s), followed by the gradual infusion of the experimental solution at a rate tailored to the experiment (here, 0.035 mL/s).

8. Image data processing and analysis

1. Bin image data into 64 x 64 pixels.
2. Determine hand-drawn regions of interest (ROIs) using ImageJ. Refer to the mouse brain atlas to designate ROIs as the frontal area (M2), the somatosensory area including the Barrel (Somato), the occipital area (Visual), and the retrosplenial region (RSC).
3. Use the MATLAB function **ReadImageJROI** to extract the coordinates corresponding to the ROIs. Access the MATLAB function through the provided link: https://jp.mathworks.com/matlabcentral/fileexchange/32479-readimagejroi
4. Compute the average rate of fluorescence intensity change within the ROI using MATLAB.
    1. Define the fluorescence intensity change rate (ΔF/F) with equation (**1**):

    $$\Delta F/F = (F_t - F_0)/F_0 \quad (1)$$

    Where F_t represents the fluorescence intensity value at a specific time and the average intensity value from the start of recording until 50 s into the injection is denoted as F_0.
5. Account for the delay in the injection solution reaching the organ. Use the average intensity value spanning the three seconds post injection as a baseline. Target waveforms surpassing the baseline intensity value + 1 SD for analysis if they occur 3 s or later post injection.

Representative Results

Transcranial cortex wide Ca^{2+} imaging with an isoflurane-anesthetized G7NG817 mouse

We created the catheter following the procedure illustrated in **Figure 1**. After carefully identifying the position of the stomach, we attached the catheter to that location (**Figure 1**). After allowing sufficient recovery time following catheter insertion (approximately 48 h), we measured spontaneous neural activity under mild isoflurane anesthesia (0.8-1.0%) to establish the baseline fluorescence intensity changes for subsequent intestinal stimulation observations. As a result, we confirmed the random Ca^{2+} oscillation patterns that spanned the entire cortex (**Figure 2A**). **Figure 2** provides representative examples of spontaneous brain activity, with the catheters inserted beforehand. We defined the time of the first observable Ca^{2+} transient peak in the M2 region following the injection as 0.0 s. The pseudo color representation displayed the peak of this Ca^{2+} transient as the maximum value, with the mean value plus one standard deviation (1 SD) as the minimum value. It was clear that the left and right hemispheres displayed synchronous activity in all regions.

Next, we established ROIs to characterize the waves within each functional area. As shown in **Figure 2B**, we presented **the temporal changes in fluorescence intensity rate for each ROI** (**Figure 2B**). These observed surface Ca^{2+} oscillations followed a burst suppression pattern, alternating between periods of low activity and high-amplitude fluorescence changes. This activity pattern aligns with previous findings that simultaneously measured cortical surface EEG and Ca^{2+} dynamics[26].

Despite global or regional surface Ca^{2+} fluctuations between suppression and burst states, the specific cortical region

initiating the calcium surge can differ. As previously reported, when a signal stimulates a local cortical region, the area is expected to activate, subsequently driving a global shift in the cortical state[27,28].

Changes in cortex Ca^{2+} dynamics after intragastric glucose injection

Next, to elucidate how glucose or water administration influences cortical activity, we monitored cortex wide Ca^{2+} dynamics during and after the injection. As a result, we found alterations in cortical Ca^{2+} dynamics following intragastric glucose injection. In contrast to the spontaneous activity illustrated in diverse regions of cortical activation, we observed immediate activation in the prefrontal area or the secondary motor cortex (M2) upon direct gut injection of glucose via the catheter, an effect not induced by intragastric water injection (**Figure 3A-C**). Moreover, we observed that these transient, prominent Ca^{2+} events tended to occur continuously over approximately 10 s following intragastric glucose injection. Such persistent phenomena were not apparent when water was administered (**Figure 3D-F**).

The Ca^{2+} events in each ROI were characterized by calculating the ratio of fluorescence intensity change ratio, using the auditory cortex (Reference) as a reference, at the first peak occurring within 4-8 s after the completion of glucose administration. As a result, a significant change was observed when glucose was injected after comparing the response in the M2 region using the auditory cortex as a reference before and after injection.

In contrast, no such change was observed when water was injected (**Figure 3G**, water N = 7: before vs. injection, 2.38 ± 2.53 vs. 2.05 ± 1.84, $p > 0.05$; glucose N = 7: before vs. injection, 2.48 ± 0.97 vs. 3.76 ± 2.76, $p < 0.01$, Wilcoxon signed-rank test). Next, defining the activation levels in each cortical region by the ratio of the value of after injection to before injection, a significant difference was observed only in the M2 region (**Figure 3H**, M2: 0.92 ± 0.89 vs. 1.30 ± 0.32, $p = 0.006$; Somato: 0.95 ± 0.076 vs. 1.04 ± 0.13, $p = 0.27$; Visual: 0.92 ± 0.3 vs. 1.00 ± 0.06, $p = 0.89$; RSC: 0.97 ± 0.27 vs. 1.10 ± 0.27, $p = 0.60$, *t*-test).

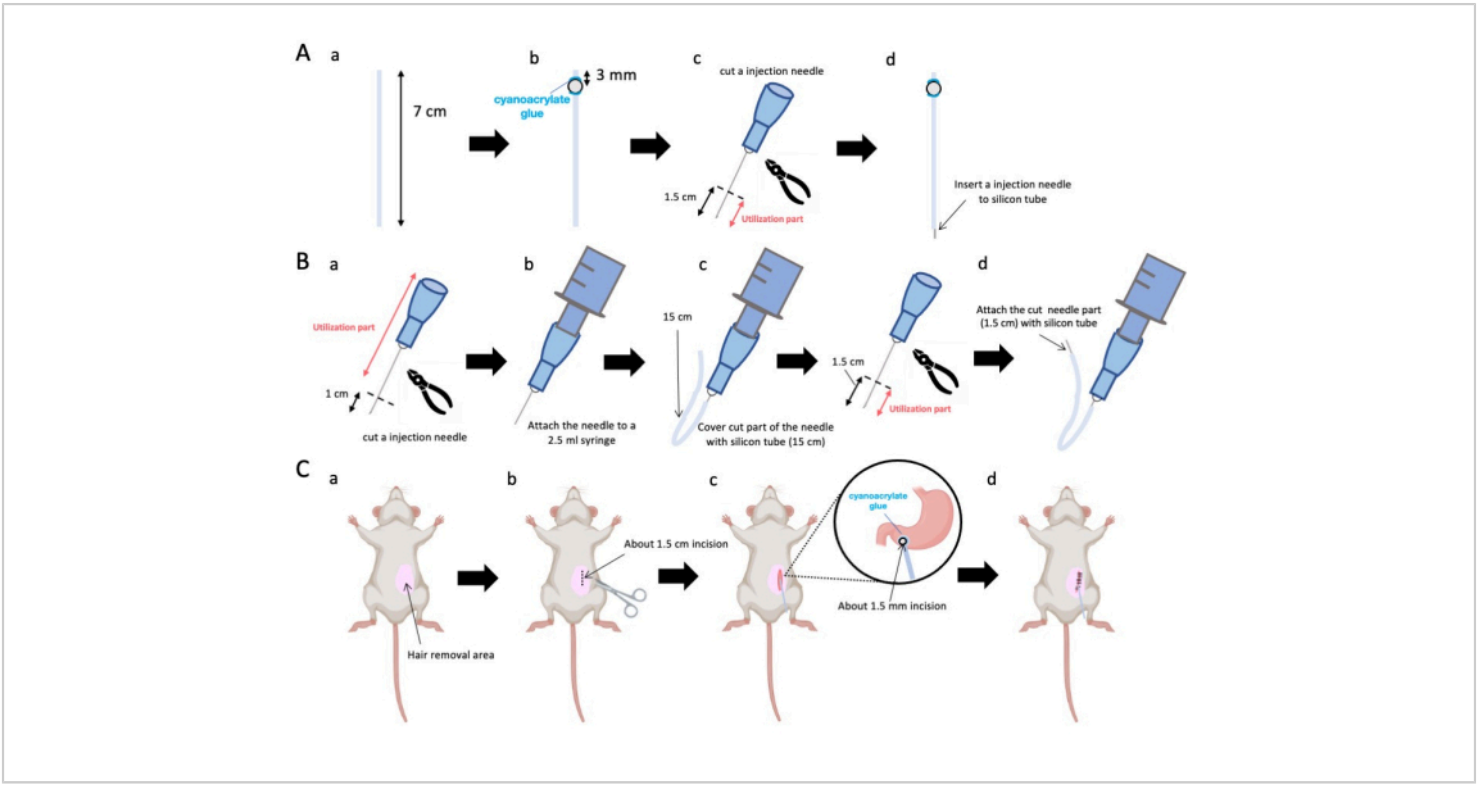

Figure 1: Overview of the method. (**A**) Catheter creation: (a) Cut the silicon tube. (b) Affix a plastic bead to the silicon tube using medical cyanoacrylate glue. (c) Cut the 23 G needle 1.5 cm from the tip. (d) Attach the cut end of the needle to the silicon tube. (**B**) Injector assembly: (a) Trim a 23 G injection needle by 1 cm. (b) Connect the trimmed injection needle to a 2.5 mL syringe. (c) Sheath the cut section of the injection needle with a silicon tube. (d) Cut the 23 G needle 1.5 cm from the tip. (e) Attach the cut end of the needle to the silicon tube. (**C**) Surgical procedure: (a) Depilate the surgical area. (b) Incise the skin and the abdominal wall to a length of approximately 1.5 cm. (c) Create a small perforation (around 1.5 mm in diameter) in the pyloric antrum using scissors and insert the catheter (silicon tube). Secure the catheter to the pyloric antrum using medical cyanoacrylate glue. (d) Stitch the abdominal wall and skin using 5/0 silk suture material and needle. Please click here to view a larger version of this figure.

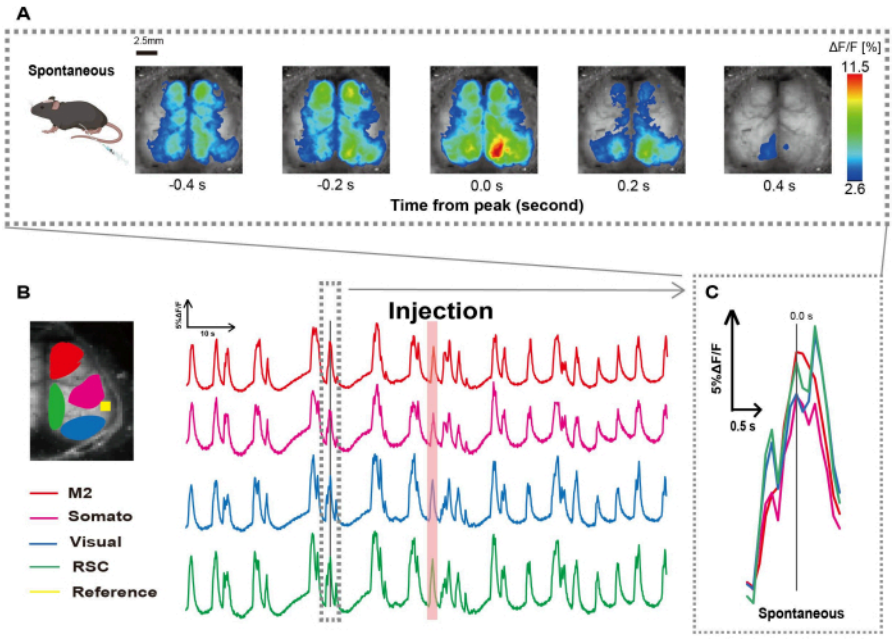

Figure 2: Spontaneous cortex wide Ca^{2+} oscillations in G7NG817 mice with an attached catheter. (**A**) A representative example of cortex wide Ca^{2+} oscillations displayed at 0.2 s intervals. Changes in fluorescence intensity are represented with a pseudo color overlay. The time window encircled by the dashed line in **B** shows the first appearing Ca^{2+} transient, with its peak set as time 0. The pseudo color representation uses the peak of that Ca^{2+} transient as the maximum value and the mean +1 SD as the minimum value. (**B**) Time series changes in fluorescence intensity for each ROI in the example. Line colors correspond to different cortical areas: red represents M2; magenta represents the somatosensory area (Somato); blue represents the visual area (Visual); and green represents the retro splenial region. Salmon colored strip shows the injection time. (**C**) A single peak within the dashed outline is isolated and displayed in an enlarged view. Abbreviations: SD = standard deviation; ROI = region of interest; RSC = retro splenial region. Please click here to view a larger version of this figure.

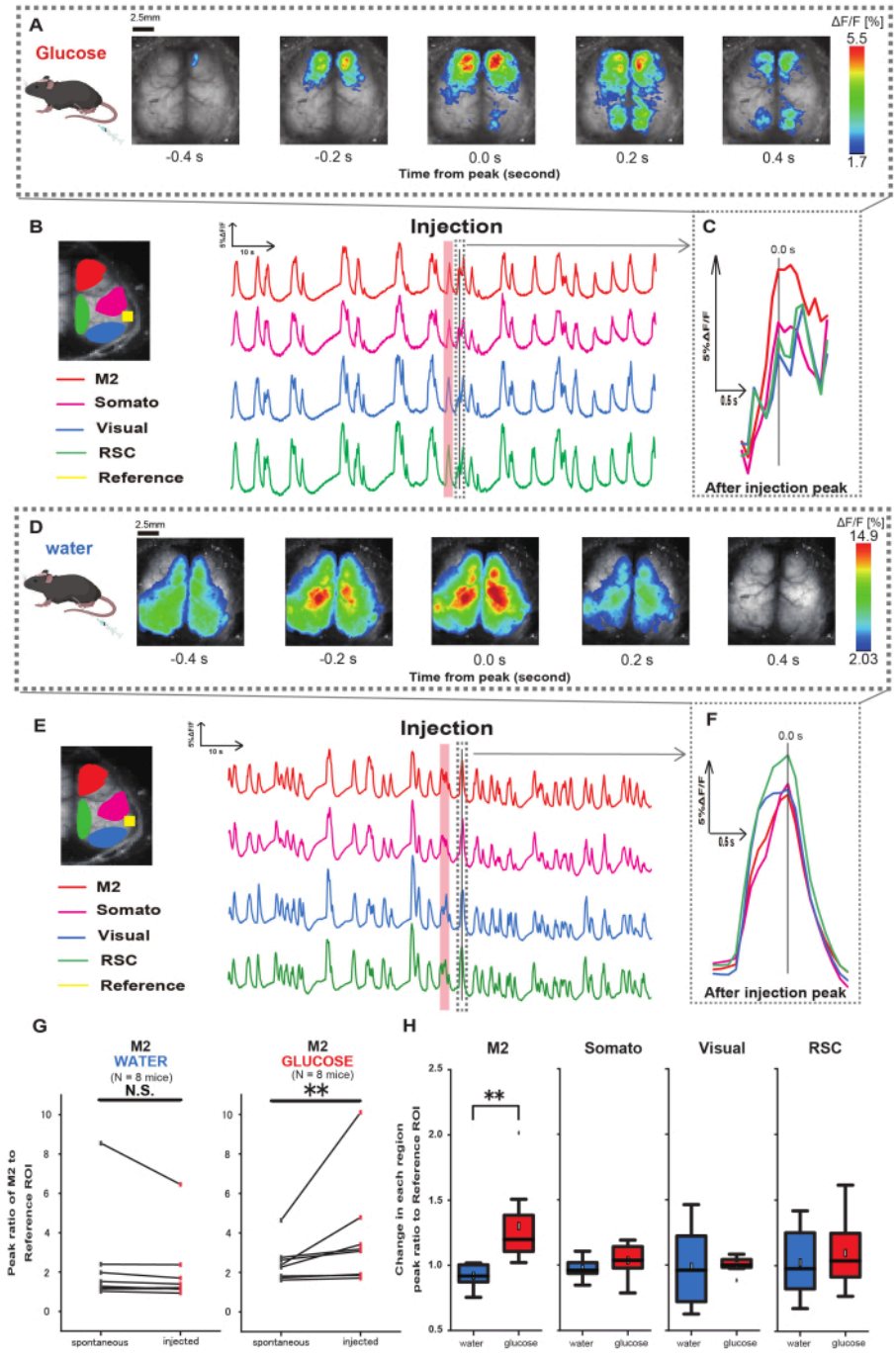

Figure 3: Cortex wide Ca^{2+} response during/after glucose or water injection. (**A**) A representative example of glucose administration displayed at 0.2 s intervals. Changes in fluorescence intensity are represented with a pseudo color overlay. The time window encircled by the dashed line in **B** shows the first appearing Ca^{2+} transient after the injection, with its peak set as time 0. The pseudo color representation is based on the peak of the first Ca^{2+} transient after injection as the maximum value and the mean +1 SD as the minimum value. (**B**) Time series changes of fluorescence intensity for each ROI

in the example. Line colors correspond to different cortical areas: red represents M2, magenta represents the somatosensory area (Somato), blue represents the visual area (Visual), and green represents the retro splenial region. (**C**) A single peak within the dashed outline is isolated and displayed in an enlarged view. Analyze target calcium wave is the earliest wave that appeared within 4-8 s after injection. (**D**) A representative example of water injection as glucose control data. (**E**) Time series changes in fluorescence intensity for each ROI in the example. Line colors are as in **B**. (**F**) A single peak within the dashed outline is isolated and displayed in an enlarged view. Analyze target calcium wave is the earliest wave that appeared within 4-8 s after injection. (**G**) Comparison of M2 spontaneous activity (before) and response after injection (injected). The average fluorescence intensity changes over 50 s before injection, and the peak response in the M2 region between 4 s and 8 s after injection was calculated, using the auditory cortex as a reference. (**H**) Comparison of activation levels in each cortical region when water or glucose was administered. The ratio of the value of after injection to before injection, as determined in **G**, was calculated for each region. N.S. represents non-significant ($p > 0.05$). ** <0.01. Error bars are defined as the standard error of the mean. Abbreviations: SD = standard deviation; ROI = region of interest; RSC = retro splenial region. Please click here to view a larger version of this figure.

Discussion

This article presents how to attach a catheter to the gut and observe transcranial cortex wide Ca^{2+} signals with transgenic mice that express a genetically encoded Ca^{2+} indicator. In this experiment, we did not get the imaging data that use a secondary wavelength of the light source. This is because the transgenic mice we employed in this study exhibit a very high fluorescence intensity change rate (~several tens of percent) in response to sensory stimuli due to the properties of the Ca^{2+} indicator protein (G-CaMP7) employed. Hence, we thought that contamination from hemodynamics was negligible. Furthermore, the neural responses we focused on occurred rapidly within a few seconds, so we considered it unnecessary to account for subsequently generated local functional hyperemia. This catheter implantation method is able to combine with other genetically modified mice to observe neuronal activity in other brain regions and on different timescales. However, if other genetically modified mice are used, the control experiment described above should be performed.

This method of attaching the catheter to the gut is suitable for single-dose injection at low cost and is easy and less invasive than the method proposed earlier[29]. Traditionally, absorbent cotton is applied to the digestive organ and sutured. However, suturing can impair post-operative recovery in mice. Therefore, we adopted the method of attaching. The reason that we chose plastic beads is they adhered better to the silicone with the cyanoacrylate glue we use.

It has traditionally been postulated that the brain perceives glucose based on the escalation in plasma blood glucose levels and the concomitant hormone release. Consequently, the brain requires several minutes to hours to detect glucose following its absorption from the gut[4]. Some research has suggested that gut sensing controls mice's taste preference in addition to oral sweet taste reception[1,3,17,22]. As an illustrative example, researchers have provided evidence that intragastric (IG) glucose-paired flavored non-nutritive solution and IG nonmetabolizable α-methyl-d-glucopyranoside (MDG)-paired flavored non-nutritive solution can elicit preference for each flavored non-nutritive solution

compared to the IG water-paired group. As intraperitoneal glucose injection did not stimulate non-nutritive solution intake[30], it was anticipated that gut nutrient sensing would play a crucial role in the food choices of the mice[1,19,22].

A recent study has revealed the presence of an electrically excitable cell in the gut, referred to as a "Neuropod cell," which employs molecular receptors to detect and transduce sensory stimuli onto a vagus nerve via a glutamatergic synapse. While previous studies have primarily focused on the role of GLP-1 in controlling mice's food feeding, recent investigations have demonstrated that vagus nerve activation by neuropod cells modulates mouse appetite. The vagus nerve subsequently activates the Nucleus Tractus Solitarius, leading to the subsequent activation of dopaminergic neurons[19]. However, it is unknown if dopaminergic neuron activation also activates the cortex. To categorize cerebral responses following intragastric glucose infusion, we refined the catheter attachment technique for imaging purposes. When employing this technology, it is imperative to exercise caution to prevent organ damage, with particular regard to the liver, which is susceptible to injury during the manipulation required to ascertain the stomach's location.

Our findings indicate that intragastric glucose injection activates the prefrontal cortex within seconds. However, intragastric glucose administration initiates multiple signaling pathways simultaneously, such as hormonal routes, the vagus nerve, and the spinal afferent nerve. These signals are processed in the brain stem on different timescales. Therefore, future studies should explore how these intricate signals are processed and integrated within the brain.

Moreover, the BAC GLT-1-G-CaMP7 transgenic mouse line we employed in the present study expresses the Ca^{2+} sensor, G-CaMP7, in both neurons and astrocytes. In principle, the prefrontal Ca^{2+} elevation obtained by transcranial cortex wide Ca^{2+} imaging is derived from neurons and/or astrocytes. However, since astrocytes express dopamine receptors if dopamine signaling is involved, it suggests the potential activation of astrocytic IP_3/Ca^{2+} signaling. Since astrocytic IP_3/Ca^{2+} signaling regulates synaptic plasticity, it may also play an important role in changes in sucrose preference and alterations in feeding behavior after glucose reception. Consequently, imaging at cellular resolution using two-photon microscopy would be required to identify whether the response observed in the prefrontal cortex following glucose administration originated from neurons or astrocytes in future studies. Another effective method involves observing cell-specific Ca^{2+} indicator expression in mice using adeno-associated virus (AAV) through fiber photometry. Furthermore, it is necessary to verify, using electrophysiological techniques, whether the glucose stimulus to the intestine genuinely stimulated the vagus nerve. If neuropod cells are transmitting signals to the vagus nerve by receiving glucose, we anticipate no response from the vagus nerve when an SGLT-1 inhibitor is administered. Finally, validation using various dopamine receptor antagonists would be necessary to confirm whether the vagus nerve projections to the Nucleus Tractus Solitarii (NTS) activated dopaminergic neurons, increasing prefrontal cortex Ca^{2+} signals. Overall, this system enables a comprehensive investigation of the rapid neural transmission effects from the gut to the brain. It presents a highly promising methodology that could potentially elucidate mechanisms, such as how stress alters sucrose preference regarding gut-brain interactions.

Disclosures

The authors have no conflicts of interest to disclose.

Acknowledgments

This work was supported by Ochanomizu University, KAKENHI grants (18K14859, 20K15895), JST FOREST Program, Grant Number JPMJFR204G, Research Foundation for Opto-Science and Technology, Kao Research Council for the Study of Healthcare Science, The Japan Association for Chemical Innovation, and TERUMO life science foundation. The author thanks Dr. Takashi Tsuboi, Kazuki Harada, and Akiyo Natsubori for their supervision of the experiments. The author also thanks members of the laboratory for their support.

References

1. Buchanan, K. L. et al. The preference for sugar over sweetener depends on a gut sensor cell. *Nature Neuroscience.* **25** (2), 191-200 (2022).
2. Reimann, F. Molecular mechanisms underlying nutrient detection by incretin-secreting cells. *International Dairy Journal.* **20** (4), 236-242 (2010).
3. Kreuch, D. et al. Gut mechanisms linking intestinal sweet sensing to glycemic control. *Frontiers in Endocrinology.* **9**, 741 (2018).
4. Gorboulev, V. et al. Na(+)-D-glucose cotransporter SGLT1 is pivotal for intestinal glucose absorption and glucose-dependent incretin secretion. *Diabetes.* **61** (1), 187-196 (2012).
5. Harada, N., Inagaki, N. Role of sodium-glucose transporters in glucose uptake of the intestine and kidney. *Journal of Diabetes Investigation.* **3** (4), 352-353 (2012).
6. Kaelberer, M. M., Rupprecht, L. E., Liu, W. W., Weng, P., Bohórquez, D. V. Neuropod cells: The emerging biology of gut-brain sensory transduction. *Annual Review of Neuroscience.* **43**, 337-353 (2020).
7. Stanley, S., Wynne, K., McGowan, B., Bloom, S. Hormonal regulation of food intake. *Physiological Reviews.* **85** (4), 1131-1158 (2005).
8. Larsen, P. J., Tang-Christensen, M., Jessop, D. S. Central administration of glucagon-like peptide-1 activates hypothalamic neuroendocrine neurons in the rat. *Endocrinology.* **138** (10), 4445-4455 (1997).
9. Alhadeff, A. L., Rupprecht, L. E., Hayes, M. R. GLP-1 neurons in the nucleus of the solitary tract project directly to the ventral tegmental area and nucleus accumbens to control for food intake. *Endocrinology.* **153** (2), 647-658 (2012).
10. Raybould, H. E. Gut chemosensing: interactions between gut endocrine cells and visceral afferents. *Autonomic Neuroscience: Basic & Clinical.* **153** (1-2), 41-46 (2010).
11. Routh, V. H. Glucose-sensing neurons: are they physiologically relevant? *Physiology & Behavior.* **76** (3), 403-413 (2002).
12. Secher, A. et al. The arcuate nucleus mediates GLP-1 receptor agonist liraglutide-dependent weight loss. *The Journal of Clinical Investigation.* **124** (10), 4473-4488 (2014).
13. Williams, E. K. et al. Sensory neurons that detect stretch and nutrients in the digestive system. *Cell.* **166** (1), 209-221 (2016).
14. Borgmann, D. et al. Gut-brain communication by distinct sensory neurons differently controls feeding and glucose metabolism. *Cell Metabolism.* **33** (7), 1466-1482.e7 (2021).

15. Krashes, M. J. et al. Rapid, reversible activation of AgRP neurons drives feeding behavior in mice. *The Journal of Clinical Investigation.* **121** (4), 1424-1428 (2011).
16. Aponte, Y., Atasoy, D., Sternson, S. M. AGRP neurons are sufficient to orchestrate feeding behavior rapidly and without training. *Nature Neuroscience.* **14** (3), 351-355 (2011).
17. Zhang, L., Han, W., Lin, C., Li, F., de Araujo, I. E. Sugar metabolism regulates flavor preferences and portal glucose sensing. *Frontiers in Integrative Neuroscience.* **12**, 57 (2018).
18. Goldstein et al. Hypothalamic detection of macronutrients via multiple gut-brain pathways. *Cell Metabolism.* **33** (3), 676-687.e5 (2021).
19. Fernandes, A. B. et al. Postingestive modulation of food seeking depends on vagus-mediated dopamine neuron activity. *Neuron.* **106** (5), 778-788.e6 (2020).
20. Kaelberer, M. M. et al. A gut-brain neural circuit for nutrient sensory transduction. *Science (New York, N.Y.).* **361** (6408), eaat5236 (2018).
21. Bohórquez, D. V. et al. Neuroepithelial circuit formed by innervation of sensory enteroendocrine cells. *The Journal of Clinical Investigation.* **125** (2), 782-786 (2015).
22. Tan, H.-E. et al. The gut-brain axis mediates sugar preference. *Nature.* **580** (7804), 511-516 (2020).
23. Wang, D. et al. Whole-brain mapping of the direct inputs and axonal projections of POMC and AgRP neurons. *Frontiers in Neuroanatomy.* **9**, 40 (2015).
24. Yamada, S., Wang, Y., Monai, H. Transcranial cortex-wide Ca2+ imaging for the functional mapping of cortical dynamics. *Frontiers in Neuroscience.* **17**, 1119793 (2023).
25. Monai, H. et al. Calcium imaging reveals glial involvement in transcranial direct current stimulation-induced plasticity in mouse brain. *Nature Communications.* **7** (1), 11100 (2016).
26. Ferron, J.-F., Kroeger, D., Chever, O., Amzica, F. Cortical Inhibition during Burst Suppression Induced with Isoflurane Anesthesia. *The Journal of Neuroscience.* **29** (31), 9850-9860 (2009).
27. Ming, Q. et al. Isoflurane-induced burst suppression is a thalamus-modulated, focal-Onset rhythm with persistent local asynchrony and variable propagation patterns in rats. *Frontiers in Systems Neuroscience.* **14**, 599781 (2021).
28. Schwalm, M. et al. Functional states shape the spatiotemporal representation of local and cortex-wide neural activity in mouse sensory cortex. *Journal of Neurophysiology.* **128** (4), 763-777 (2022).
29. Ueno, A. et al. Mouse intragastric infusion (iG) model. *Nature Protocols.* **7** (4), 771-781 (2012).
30. Zukerman, S., Ackroff, K., Sclafani, A. Post-oral glucose stimulation of intake and conditioned flavor preference in C57BL/6J mice: A concentration-response study. *Physiology & Behavior.* **109**, 33-41 (2013).